Acta Oceanol. Sin., 2022, Vol. 41, No. 5, P. 1–11
https://doi.org/10.1007/s13131-021-1879-y
http://www.aosocean.com
E-mail: ocean2@hyxb.org.cn

Numerical investigation of the South China Sea deep circulation

Shengquan Tang[1], Xueen Chen[1]*, Zhi Zeng[1, 3], Xin Liu[2]

[1] College of Oceanic and Atmospheric Sciences, Ocean University of China, Qingdao 266100, China

[2] Shandong Computer Science Center (National Supercomputer Center in Jinan), Qilu University of Technology (Shandong Academy of Sciences), Jinan 250014, China

[3] College of Meteorology and Oceanography, National University of Defense Technology, Changsha 410073, China

Received 15 April 2021; accepted 29 June 2021

Abstract

Based on a two-level nested model from the global ocean to the western Pacific and then to the South China Sea (SCS), the high-resolution SCS deep circulation is numerically investigated. The SCS deep circulation shows a basin-scale cyclonic structure with a strong southward western boundary current in summer (July), a northeast-southwest through-flow pattern across the deep basin without a western boundary current in winter (January), and a transitional pattern in spring and autumn. The sensitivity model experiments illustrate that the Luzon Strait deep overflow is the main factor controlling the seasonal variation in the SCS deep circulation. The SCS surface wind can significantly influence the SCS deep circulation in winter. The Luzon Strait deep overflow transport from the Pacific into the SCS ranges from 0.68×10^6 m^3/s to 1.83×10^6 m^3/s, reaching its maximum in summer (July, up to 1.83×10^6 m^3/s), less in autumn and winter, and the minimum in spring (May, 0.68×10^6 m^3/s). In summer, the strong Luzon Strait deep overflow dominates the SCS deep circulation when the role of the SCS surface wind is small. In winter, the weaker Luzon Strait deep overflow and SCS surface wind jointly drive the SCS deep circulation into a northeast-southwest through-flow pattern. The potential vorticity (PV) dissipation in the SCS deep basin reaches its maximum (–0.122 m^2/s^2) in May and its minimum (–0.380 m^2/s^2) in July.

Key words: South China Sea, deep sea circulation, deep overflow, surface wind, potential vorticity

Citation: Tang Shengquan, Chen Xueen, Zeng Zhi, Liu Xin. 2022. Numerical investigation of the South China Sea deep circulation. Acta Oceanologica Sinica, 41(5): 1–11, doi: 10.1007/s13131-021-1879-y

1 Introduction

The South China Sea (SCS) is the largest marginal sea of the North Pacific (Chao et al., 1996; Wang et al., 2011). In the SCS deep basin, the Luzon Strait deep channel is the only channel connecting the SCS and the Pacific Ocean (Qu et al., 2006; Sun et al., 2017; Wang et al., 2011).

Influenced by the water exchange through the Luzon Strait and the East Asian monsoon, the climatological annual mean SCS circulation presents a "sandwich" structure in the vertical direction (Yuan, 2002). The climatological annual mean upper water and deep water of the SCS are cyclonic circulations, and the climatological annual mean intermediate water is an anticyclonic circulation (Gan et al., 2006, 2016; Li and Qu, 2006; Liu and Gan, 2017; Tian et al., 2006; Shu et al., 2014; Wang et al., 2012, 2016; Yuan, 2002; Zhu et al., 2016). The SCS deep circulation results from interactions among multiscale dynamic processes and complex topography and refers to the circulation system at more than 2 000 m depth in the SCS basin (Tian and Qu, 2012). There is a persistent density difference between the SCS water and the Pacific water below 1 500 m depth (the density is higher in the Pacific than in the SCS below 1 500 m), which is identified as a baroclinic pressure gradient driving flow from the Pacific into the SCS (Qu et al., 2006). After entering the SCS deep basin, the Luzon Strait deep overflow turns northwestward, forming an annual mean basin-scale cyclonic circulation (Yuan, 2002; Qu et al., 2006; Wang et al., 2011). Lan et al. (2013) also suggested that the most obvious features of the climatological annual mean SCS deep circulation are basin-scale cyclonic gyre and western intensification.

The mechanisms of the SCS deep circulation are complex. The water transported into the SCS deep basin through the Luzon Strait deep channel tends to follow potential vorticity (PV) contours, which are approximately parallel to the local isobaths (Pedlosky, 1982, 1996; Qu et al., 2006). Therefore, the pattern of the annual mean potential density and PV distribution in the SCS deep basin are consistent with the cyclonic circulation (Li and Qu, 2006; Qu et al., 2006; Wang et al., 2011). Lan et al. (2013) first used the PV-integral constraint to discuss the dynamic mechanisms of the SCS deep circulation. However, the spatial and temporal pattern of PV dissipation in the SCS deep basin remains unclear. As we discussed above, previous studies of SCS deep circulation have mainly focused on its annual mean characteristics, while its seasonal variation has received little attention. Using a model resolution of 0.5°×0.5°, Lan et al. (2015) first compared the SCS deep circulation in summer with that in winter and found that the SCS deep circulation is cyclonic in summer and weakly cyclonic in winter. Lan et al. (2015) also considered the effect of the whole Luzon Strait exchange on the SCS deep circulation by clos-

Foundation item: The National Key Research and Development Program of China under contract No. 2021YFF0704002; the Aoshan Science and Technology Innovation Program of Pilot National Laboratory for Marine Science and Technology (Qingdao) under contract No. 2018ASKJ01-04.

*Corresponding author, E-mail: xchen@ouc.edu.cn

ing the whole Luzon Strait in their model and found that the SCS deep circulation is strong and anti-cyclonic in both summer and winter after closing the whole Luzon Strait. However, the closure of the whole Luzon Strait also removes the upper flow and intermediate flow across the Luzon Strait, so the sole influence of the Luzon Strait deep overflow on the SCS deep circulation cannot be determined. We speculate that due to the relatively coarse model resolution, the Luzon Strait deep channel cannot be well resolved numerically by a model resolution of 0.5°×0.5°; thus, designing a sensitivity model experiment that blocks only the Luzon Strait deep overflow requires a higher model resolution.

In summary, the annual mean SCS deep circulation is commonly thought to be cyclonic. However, does the SCS deep circulation have a strong seasonal variation? If so, what is responsible for such variations? As discussed by Lan et al. (2015), the SCS deep circulation will reverse its rotational direction without the whole Luzon Strait water exchange. However, if we only switch off the Luzon Strait deep overflow, will the SCS deep circulation still reverse its rotational direction as it does without the whole Luzon Strait exchange? If not, how will the SCS deep circulation respond, and what is the explanation? In this work, we try to resolve the above mentioned questions by employing a higher resolution model, which is able to describe the model topography difference between switching the Luzon Strait deep overflow on and off. Additionally, a sensitivity model experiment of switching off the local surface wind over the SCS is designed for further examination of the wind forcing role in the SCS deep circulation.

The present paper is organized as follows. A brief introduction to the validation data and model configuration is given in Section 2. In Section 3, the model results and validation are introduced. The PV dissipation of the SCS deep basin is estimated in Section 4. The sensitivity model experiments are given in Section 5 to study the factors of the SCS deep circulation seasonality. The conclusions are summarized in Section 6.

2 Data and model configuration

2.1 *Data*

The data used in this paper include simple ocean assimilation data (SODA), i.e., ocean reanalysis data (Carton et al., 2005; Carton and Giese, 2008). SODA uses an ocean model based on Geophysical Fluid Dynamics Laboratory MOM2 physics and assimilates data including temperature and salinity profiles from the World Ocean Atlas (MBT, XBT, CTD, and station data), as well as additional hydrography, sea surface temperature, and altimeter sea level (Carton et al., 2000). The SODA model, integrated from 1871, therefore, is thought to reach equilibrium states in the deep ocean.

In our study, the version number of the SODA product we used is SODA2.2.4. The model used to produce SODA2.2.4 has an average horizontal resolution of 0.25°×0.4° and 40 vertical levels. Zhu et al. (2016) used SODA2.2.4 to study the seasonal variability in the meridional overturning circulation in the SCS and proved that SODA2.2.4 has good scientific value for studying SCS circulation dynamics, including deep circulation in the SCS. Therefore, considering the good scientific value, sufficient assimilation and long model integration, it is reasonable to use SODA2.2.4 as the validation model data for our model.

In our study, the SODA2.2.4 data are processed as the 41-year climatological monthly mean from January 1960 to December 2000 for our model validation. The model output of SODA2.2.4 is mapped onto a uniform 0.5°×0.5°×40-level grid.

2.2 *Model configuration*

A two-level nested model that can simulate the high-resolution SCS is used here to study the SCS deep circulation. The reasons for this model setup are described as follows. First, the Luzon deep overflow is important for simulating the SCS deep circulation. However, the Luzon deep channel is narrow, so the coarse-resolution simulation cannot sufficiently simulate the Luzon deep overflow. Therefore, a high-resolution simulation is needed to simulate the Luzon deep overflow. Second, the resolution of the model topography can also significantly affect the accuracy of simulation of the SCS deep circulation (Xie et al., 2013). Therefore, a high-resolution model is needed to fully resolve the SCS deep circulation. Third, the water characteristics in the SCS are not only influenced by local forcings but also by remote forcings from the open ocean. Therefore, a global simulation is better than a regional simulation. However, because of the high computing cost, a high-resolution global simulation is not available in our study. Therefore, this study established a two-level nested simulation, from global to the western Pacific and then to the SCS, which can fully transmit the signals from the remote ocean to the SCS and simulate the high-resolution SCS.

The model configuration is the same as that in Tang et al. (2019). Figure 1 shows the nested simulation domains and the SCS topography. The ocean model used in this work is the hybrid coordinate ocean model (HYCOM). The two-level nested simulation is from (almost) the global ocean model (1°×1°) of 60°S–54°N, 180°W–180°E to the western Pacific model (0.2°×0.2°)

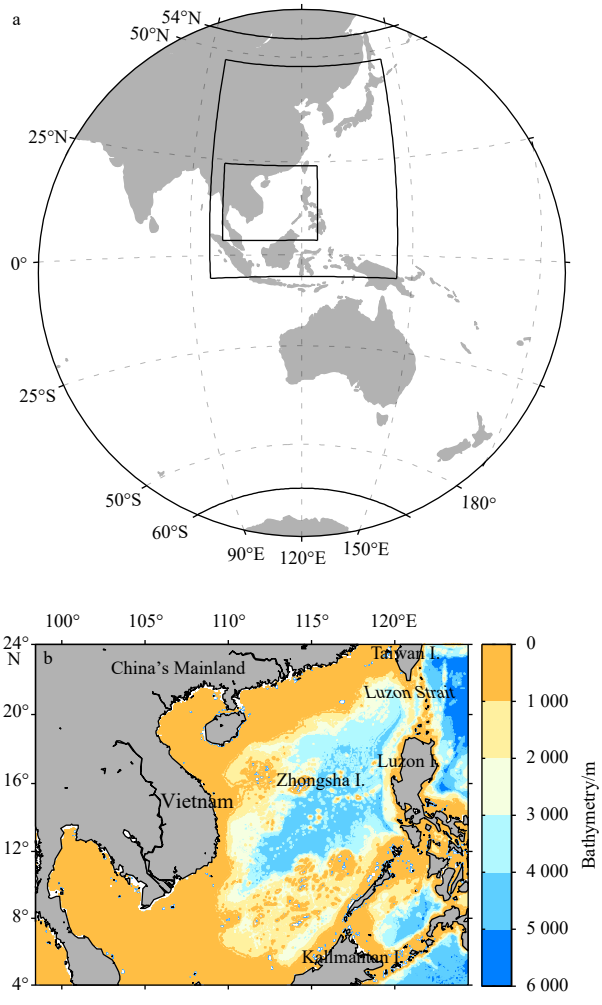

Fig. 1. The two-level nested simulation domains (a) and the bathymetry of the SCS model (b). Zhongsha Island is shown in b.

of 6°S–48°N and 95°–146°E, then to the SCS model (0.04°×0.04°) of 4°–24°N and 98.4°–124.4°E. The global ocean model is run for 50 model years, the western Pacific model is run for 25 model years, and the SCS model is run for 23 model years. The integral times of the sensitivity model experiment in Sections 4.2 and 4.3 are the same as that of the SCS model of the control run. The two-level model is forced by a monthly climatological Comprehensive Ocean-Atmosphere Data Set (COADS) with a 1°×1° grid resolution. The boundary conditions of the western Pacific model come from the (almost) global ocean model, and the boundary conditions of the SCS model come from the western Pacific model.

The total model years run in this two-level nested model is 50 model years. Hirschi et al. (2013) found that the ocean model starting from rest has strong drifts during the first 10–15 model years (which is approximately 1×10^6 m^3/s per year) but has smaller long-term drifts after this initial phase (which is approximately 2×10^6 m^3/s per century); therefore, the ocean state can be thought to reach a quasi-steady state after this initial phase. Since our model has run for 50 years, the model results reach quasi-equilibrium states, which can be used to perform the scientific analysis. To obtain the analytical results closer to equilibrium, we use the model result of the final year to perform the scientific analysis. The outputs of the daily mean in the SCS model are saved for the analysis.

Compared with the previous SCS deep circulation model, for example, Lan et al. (2015), the major advance of our model, nested HYCOM (hereinafter named NHYCOM), is the high-resolution grid configuration that also considers the global signal. Therefore, our model can simulate the Luzon Strait deep overflow in greater detail and fully consider the topography influence and global signals.

3 Model results and validation

3.1 *SCS deep circulation and its seasonal variation*

We represent the deep circulation by monthly means of velocity, vertically averaged from downward 2 000 m depth (Figs 3a–d). The NHYCOM output has similar flow patterns to the 41-year climatology from SODA (Figs 2a–d) but generally higher flow speeds: spatial average of 0.005 9 m/s in NHYCOM compared with 0.002 9 m/s SODA. In January, both models are dominated by a southwestward current flowing from northeast to southwest in the central longitudes of the basin (Figs 2a and 3a). In April and July, the basin is filled with cyclonic circulation (Figs 2b, c and 3b, c). In October, the circulation is in a transitional state that has a weaker cyclonic flow in SODA (Fig 2d). NHYCOM has a

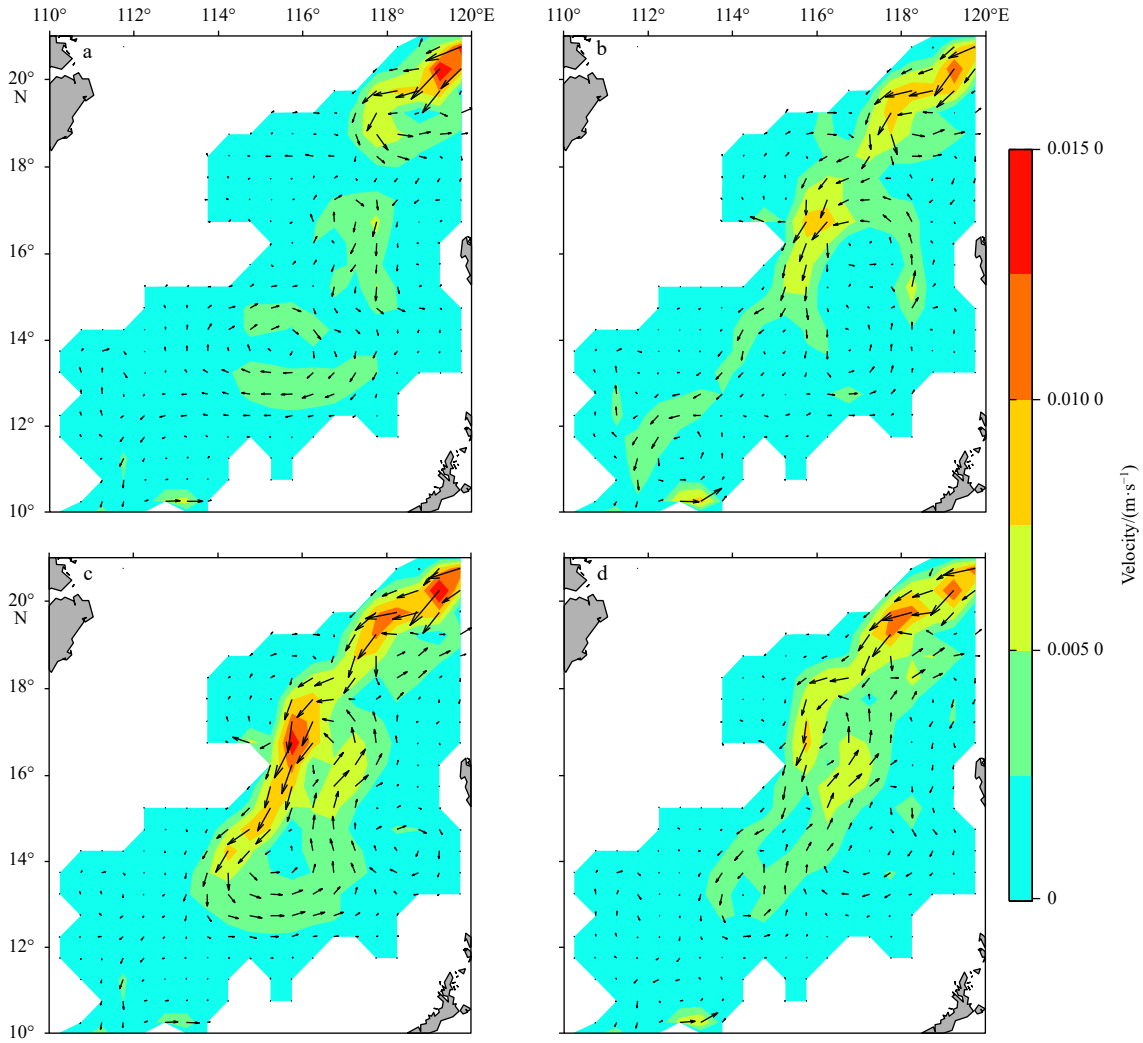

Fig. 2. The climatological monthly mean SCS deep circulation of SODA data (vertically averaged downward from 2 000 m depth) in January (a), April (b), July (c) and October (d).

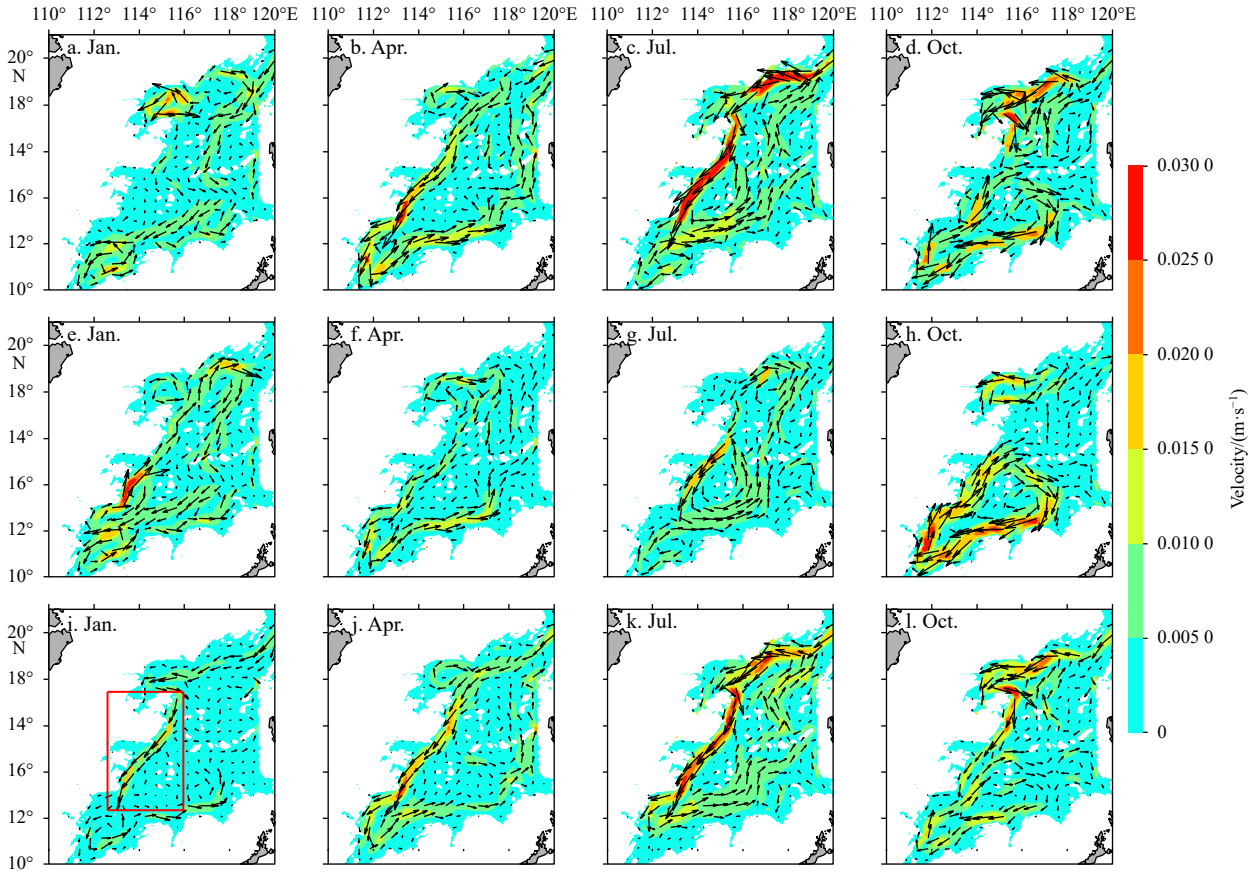

Fig. 3. The NHYCOM_produced monthly mean SCS deep circulation (vertically averaged downward from 2 000 m depth) in January, April, July and October for the control experiment (a–d), for the topography modified experiment (e–h), and for the wind sensitivity experiment (i–l). The red box in i indicates the western boundary, where compared with the control experiment, the deep circulation shows an obvious change. The current arrows are plotted approximately 4 every 2 degrees and are smoothed by averaging 81_grids around the central arrow.

more complex flow, with a cyclone in the northern part of the basin and an anticyclone in the south (Fig. 3d). The SCS deep western boundary current in spring and summer is stronger than that in autumn and winter. Using mooring data, Zhou et al. (2017) analyzed the seasonal variation in the SCS deep western boundary current and obtained similar results (see supplementary Fig. S4, Zhou et al. (2017)). The difference of the circulation strength between our model and the SODA maybe because our model uses higher gird resolution which can better simulate the SCS topography and produce more real strong deep circulation. Basing on the mooring data, the current speed of our model results is closer to the observed results.

The annual_average flow (Fig. 4) displays an overflow from the Luzon Strait. The overflow connects to a southward-flowing western boundary current. The current is part of a basin-spanning cyclone with relatively broad and slow flow in the northward-flowing limb of the gyre. This annual mean SCS deep circulation is in good agreement with previous results (Wang et al., 2011; Lan et al., 2013). In the SCS deep western boundary, the maximum annual mean velocity is up to 2.2 cm/s. The simulated SCS deep western boundary current mainly exists east of Zhongsha Island, which has been confirmed by mooring data from 2012–2014 (Zhou et al., 2017).

In conclusion, the NHYCOM reproduces the pattern and seasonal variation in the SCS deep circulation well. The SCS deep circulation is a basin-scale cyclonic structure with a strong south-

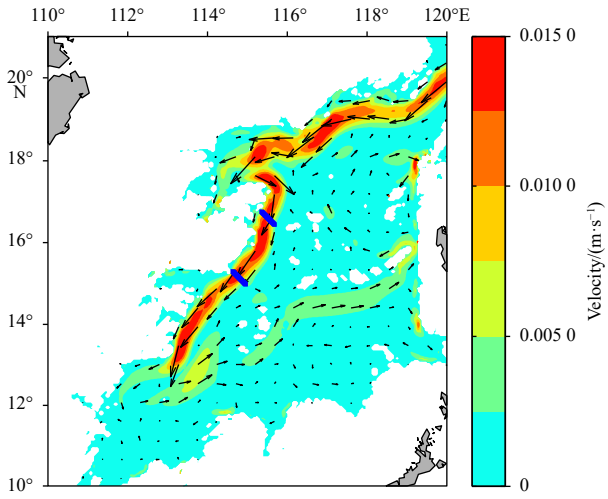

Fig. 4. The NHYCOM produced annual mean SCS deep circulation (vertically averaged downward from 2 000 m depth). The current arrows are plotted approximately 4 every 2 degrees and are smoothed by averaging 81_grids around the central arrow. The two blue sections represent the western boundary section used to calculate the deep western boundary current transport in Section 5.2.

ward deep western boundary current in summer (July); and a northeast-southwest through-flow across the central SCS deep basin without an obvious deep western boundary current in winter (January), while spring and autumn are two transitional seasons. The annual mean of the SCS deep circulation shows a cyclonic structure.

3.2 *The Luzon Strait deep overflow and its seasonal variation*

The Luzon Strait is the deepest channel connecting the SCS and Pacific. The SCS deep circulation can be closely related to the Luzon Strait deep overflow. There are two meridional ridges in the Luzon Strait. The deep water exchanges between the Pacific and the SCS through the Taltung Channel in the eastern ridge (Section TC in Fig. 5a) and Bashi Channel in the eastern ridge (Section Bsh in Fig. 5a) and three channels in the western ridge (Sections N, S1 and S2 in Fig. 5a). After entering the Luzon mainly trough through the Bashi Channel, the Pacific deep water flows southwestward along the Luzon trough and then flows into the SCS deep basin mainly through the first southern channel (Section S1 in Fig. 5a) in the western ridge. The SCS deep water partly flows back to the Luzon trough through the northern channel (Section N in Fig. 5a) in the western ridge. The transport in each channel (a positive value represents the water flowing into the SCS) shows obvious seasonal variation (Fig. 5b). The Taltung Channel transport is small and is 0.07×10^6–0.23×10^6 m^3/s. The Bashi Channel transport (sky blue line in Fig. 4b) is 0.7×10^6–2.0×10^6 m^3/s, and its transport in winter is larger than that in summer. Zhou et al. (2014) used a 3.5-year continuous mooring to show that the along-stream Bashi Channel deep overflow transport is $(0.83\pm0.46)\times10^6$ m^3/s, while Zhao et al. (2016) used three moorings equipped with 10 current meters and 7 CTDs to show that those transport is $(0.78\pm0.18)\times10^6$ m^3/s. Our NHYCOM-produced Bashi Channel deep overflow transport is slightly more than the results of Zhao et al. (2016) but comparable with the results of Zhou et al. (2014). The first southern channel in the western ridge is the main channel for the Luzon trough deep water flowing into the SCS deep basin, with a transport (red line in Fig. 5b) of 1.0×10^6–2.0×10^6 m^3/s, and its transport in summer is larger than that in winter. The second southern channel (Section S2 in Fig. 5a) transport is small and is 0.20×10^6–0.38×10^6 m^3/s. The SCS deep water partly flows back into the Luzon Trough through the northern channel in the western ridge, with a Transport (blue line in Fig. 5b) of 0.5×10^6–0.2×10^6 m^3/s. Zhao et al. (2014) used observed mooring data to prove that the SCS deep water partly flows back to the Luzon trough through the northern channel of the western ridge.

The total transport of the northern and first southern channels and second southern channels in the western ridge (gray line) indicates the total deep water exchange between the SCS deep basin and the deep Pacific, which is approximately 0.68×10^6–1.83×10^6 m^3/s and reaches its maximum in summer (July, up to 1.83×10^6 m^3/s) and minimum in spring (May, 0.68×10^6 m^3/s). The estimated transport of the Luzon Strait deep overflow simulated in this study is similar to that of previous work (Chang et al., 2010; Tian et al., 2006; Qu et al., 2006).

In summary, the Bashi Channel and the southern channel in the western ridge are the main channels for the Pacific deep water flowing into the SCS deep basin. There is obvious seasonal variation in the Luzon Strait deep overflow which is largest in summer, less in autumn and winter, and smallest in spring.

4 PV dissipation in the SCS deep basin

Circulation must satisfy many types of integral constraints, such as mass, energy, and PV (e.g., Yang, 2005). When there is a net inflow at the boundary of the deep basin, it will bring the net PV to the deep basin. To ensure the PV balance, the net PV must be balanced by frictional torque, which causes a monotonic flow away from the source and along the northern and western boundary (Yang and Price, 2000). The relationship between the PV input and PV dissipation is described as follows (Yang, 2005; Yang and Price, 2007):

$$\oint_c (U_h \cdot n)\left(\frac{f+\zeta}{H}\right) \mathrm{d}s = \iint_A D_p \mathrm{d}x\mathrm{d}y, \tag{1}$$

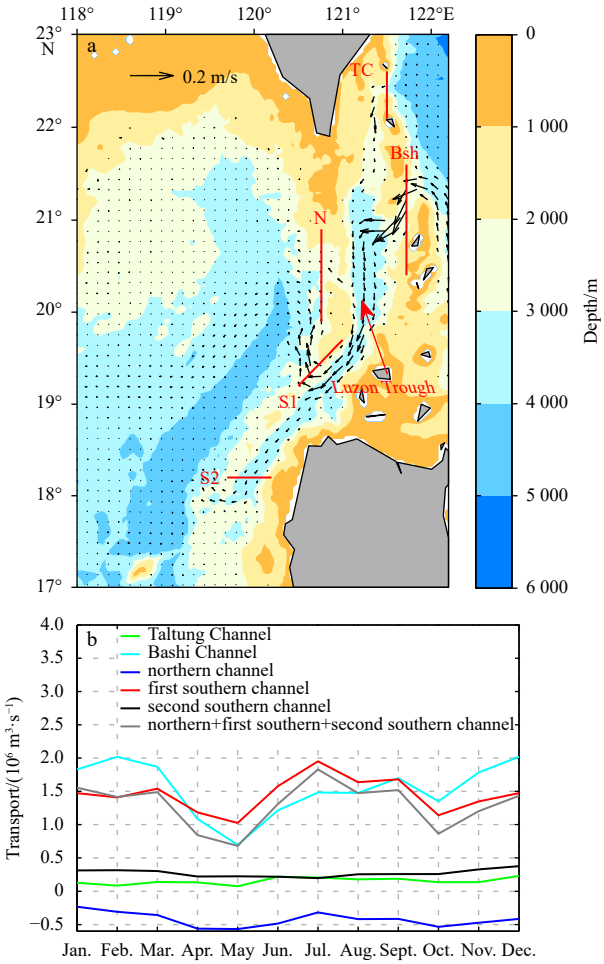

Fig. 5. The NHYCOM-produced annual mean Luzon Strait deep circulation (vertically averaged downward from 2 000 m depth) (a) and the NHYCOM-produced monthly mean transport of each channel of the deep Luzon Strait below 2 000 m depth (a positive value represents the water flowing into the SCS deep basin) (b). In a, capital "TC" indicates Taltung Channel, capital "Bsh" indicates the Bashi Channel, capital "N" indicates the northern channel in the western ridge, capital "S1" indicates the first southern channel in the western ridge, and capital "S2" indicates the second southern channel in the western ridge; in b, green line indicates the Taltung Channel transport, sky blue line indicates the Bashi Channel transport, blue line indicates the northern channel in the western ridge transport, red line indicates the first southern channel in the western ridge transport, balck line indicates the second southern channel in the western ridge transport, and gray line indicates the total transport of the northern and first southern channels and second southern channels in the western ridge.

$$\oint_c (U_h \cdot n)\left(\frac{f+\zeta}{H}\right) ds = \sum_{i=1}^{N} \frac{Qf_i}{H_i}, \quad (2)$$

$$D_p(x,y) = \frac{\partial}{\partial x}\left[\frac{A_H}{H}\nabla\cdot(H\nabla v)\right] - \frac{\partial}{\partial y}\left[\frac{A_H}{H}\nabla\cdot(H\nabla u)\right], \quad (3)$$

where n is the unit vector perpendicular to the lateral boundary, $U_h = H \cdot u_h$, $u_h = (u, v)$ is the horizontal velocity vector, H is the layer thickness of the water mass, f is the Coriolis parameter, $\zeta = v_x - u_y$ is the relative vorticity, the integral $\oint_c ds$ is along the lateral boundary, D_p is the curl of the friction, the integral $\iint_A dxdy$ is over the basin, Q is the volume transport, i is the i th opening of the lateral boundary, and A_H is the horizontal viscosity.

Lan et al. (2013) qualitatively discussed the applicability of this PV-integral constraint for SCS deep circulation. Indeed, the real ocean is more complex and nonlinear. It may impossible to ensure an accurate equality between the PV input and PV dissipation in the Oceanic General Circulation Model. However, it is still meaningful to determine how the PV dissipation of the SCS deep basin changes in space and time. In this paper, the spatial and temporal distributions of PV dissipation in the SCS deep basin are calculated, which can make us further understand the characteristics of seasonal variations in the SCS deep circulation.

The calculation method of the horizontal viscosity A_H used in this paper is provided by the HYCOM mode and is parameterized as follows (Bleck and Smith, 1990; Baraille and Filatoff, 1995):

$$A_H = \max\left\{u_d \Delta x, \lambda\left[\left(\frac{\partial u}{\partial x} - \frac{\partial v}{\partial y}\right)^2 + \left(\frac{\partial v}{\partial x} + \frac{\partial u}{\partial y}\right)^2\right]^{1/2}\Delta x^2\right\}, \quad (4)$$

where u_d is the bottom diffusion velocity and λ is a constant. In our study, $u_d = 2$ cm/s and $\lambda = 1$.

Based on the above formulations, Fig. 6 show the spatial distribution of the PV dissipation in the SCS deep basin. In winter (January), PV dissipation is not obvious at the western boundary of the SCS deep basin, corresponding to a not obvious SCS deep western boundary current. In spring (April), the PV dissipation

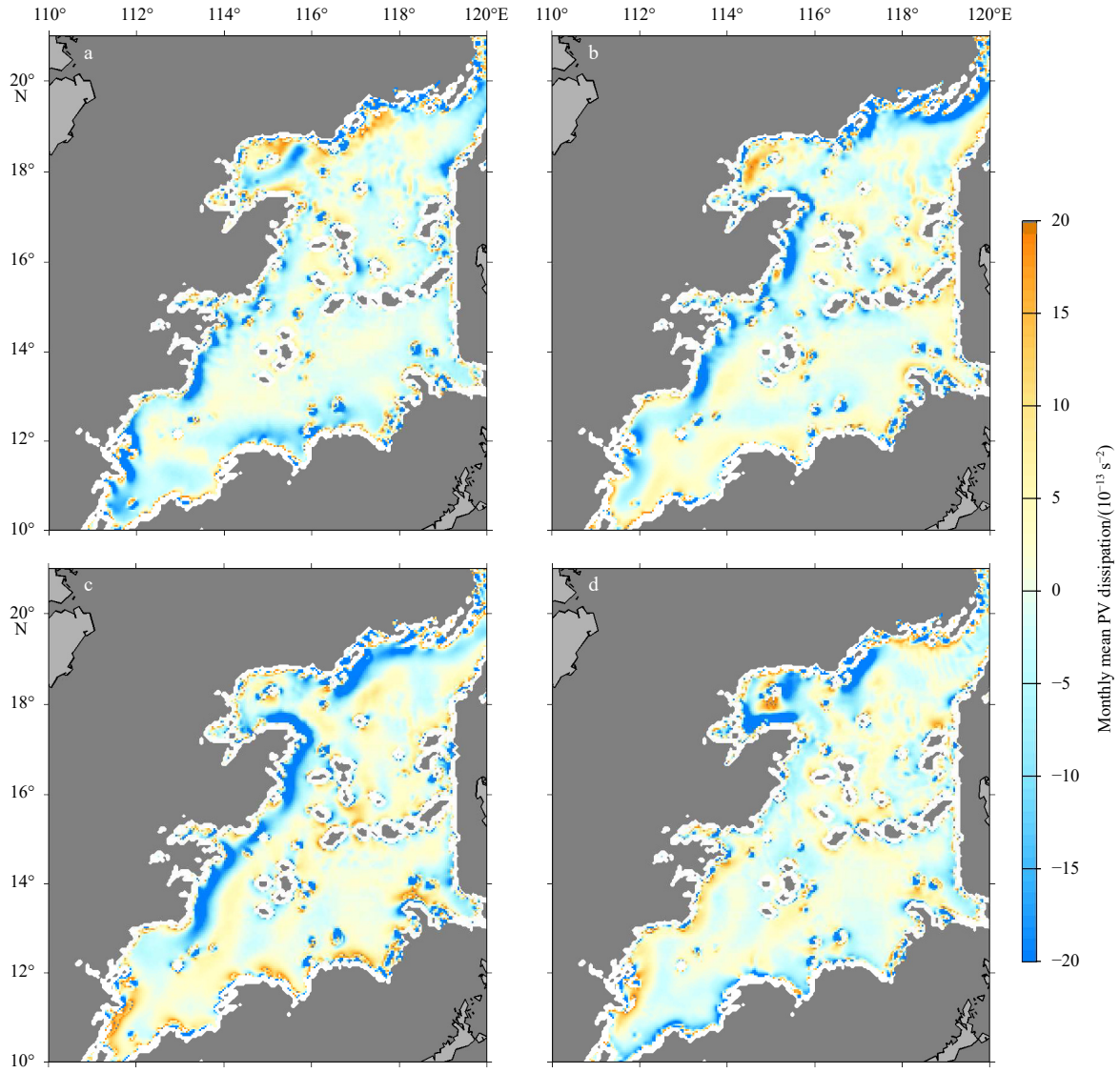

Fig. 6. The NHYCOM-produced spatial distribution of monthly mean PV dissipation in the SCS deep basin in January (a), April (b), July (c) and October (d).

occurs mainly at the western boundary of the SCS deep basin (12°–18°N), and PV dissipation at the southern part of the deep western boundary (12°–15°N) is stronger than that at the northern part of the deep western boundary (15°–18°N). In summer (July), strong PV dissipation exists at both the northern boundary and the western boundary of the SCS deep basin, corresponding to a strong SCS deep northern boundary current and the SCS deep western boundary current. In autumn (October), the PV dissipates mainly at the northern part of the western boundary (16°–18°N), as well as at the western part of the northern boundary (116°–118°E), and PV dissipation at the southern part of the western boundary is weak (13°–15°N). Table 1 shows the value of the PV dissipation for each month. The PV dissipation reaches its maximum (–0.12 m^2/s^2) in May and reaches its minimum (–0.38 m^2/s^2) in July.

Another reason for studying the PV dissipation in the SCS deep basin is that it can be used to qualitatively estimate the existence and seasonal variation of the Luzon deep overflow. According to Yang and Price (2007), the PV-integral constraint is a two-way constraint, which means that a lateral inflow of PV can determine the pattern of the basin-scale flow, but the frictional torque in the basin can also influence the transport at the boundary. In Fig. 6, we find that the PV dissipation is mainly negative in the SCS deep basin, although some positive PV dissipation appears at the northern and southern boundaries. The basin integral of PV dissipation is negative for each month and has obvious seasonal variation, with the maximum in May and minimum in July (Table 1). Based on the basin-integral PV balance, the PV advection by the Luzon deep throughflow should be positive and should also have obvious seasonal variation. Therefore, we demonstrate that the Luzon deep throughflow should be inflow from the deep Pacific into the SCS deep basin, and should have maximum transport in July and minimum transport in May. In previous work, researchers also tried different ways to estimate the existence of the Luzon deep overflow. For example, Tian et al. (2006) used observed current and hydrographic data to demonstrate the existence of the Luzon deep overflow, and Qu et al. (2006) demonstrate the Luzon deep overflow based on the persistent baroclinic pressure gradient between the Pacific and the SCS below approximately 1 500 m. Using the PV-integral constraint to qualitatively estimate the Luzon deep overflow is not contradictory to previous work since the circulation must satisfy many types of integral constraints; moreover, this constraint can more intuitively demonstrate the seasonal variation in the Luzon deep overflow. Here, we use the reverse side of the PV-integral constraint to estimate the real boundary overflow, i.e. the Luzon Strait deep overflow of the SCS deep basin. However, this reversed usage of the PV-integral constraint not only applies to SCS deep basin but can also be used for any ocean deep basin on earth.

Table 1. The PV dissipation in the SCS deep basin for each month

Month	PV dissipation/($m^2 \cdot s^{-2}$)	Month	PV dissipation/($m^2 \cdot s^{-2}$)
Jan.	–0.171	Jul.	–0.380
Feb.	–0.281	Aug.	–0.365
Mar.	–0.249	Sept.	–0.332
Apr.	–0.156	Oct.	–0.187
May	–0.122	Nov.	–0.173
Jun.	–0.221	Dec.	–0.168

5 Factors affecting the seasonality of the SCS deep circulation

5.1 *The role of the Luzon Strait deep overflow*

To explore the influence of the Luzon Strait deep overflow on the seasonal variation of the SCS deep circulation, a topography modified experiment is designed by closing the channel deeper than 1 500 m depth in the eastern ridge of the Luzon Strait (Fig. 7, inside the red box). The reason why the closed depth is 1 500 m and not another depth, is that Qu et al. (2006) demonstrate that the persistent density difference between the SCS and the Pacific driving flow from the Pacific into the SCS deep basin is mainly below approximately 1 500 m. Therefore, closing the channel deeper than 1 500 m can effectively block the Luzon deep overflow. Note that although the channel deeper than 1 500 m depth is closed, the upper limit of the Luzon Strait deep overflow is still defined as the 2 000 m depth (Zhao et al., 2014). Based on the results of Qu et al. (2006), the density difference from 1 500 m to 2 000 m is small and the obvious density difference is below 2 000 m, so the major Luzon Strait deep overflow is below 2 000 m, and the small overflow between 1 500 m and 2 000 m can be ignored. After closing the channel deeper than 1 500 m, the flow of the Pacific deep water (Fig. 5a) cannot enter the Luzon trough in the closed-channel experiment, and the Luzon Strait deep circulation almost disappears (Fig. 7).

Figures 3e–h shows the NHYCOM_produced monthly mean SCS deep circulation (vertically averaged downward from 2 000 m depth) in the topography modified experiment. The SCS deep circulation speed in the topography modified experiment is much weaker than that in the control experiment. Comparing the SCS deep circulation in the control experiment with that in the topography modified experiment, the influence of the Luzon Strait deep overflow on the SCS deep circulation also shows seasonal variation. In spring (April) and summer (July), after removing the Luzon Strait deep overflow, the SCS deep circulation pattern is unchanged, but the speed is significantly reduced. In au-

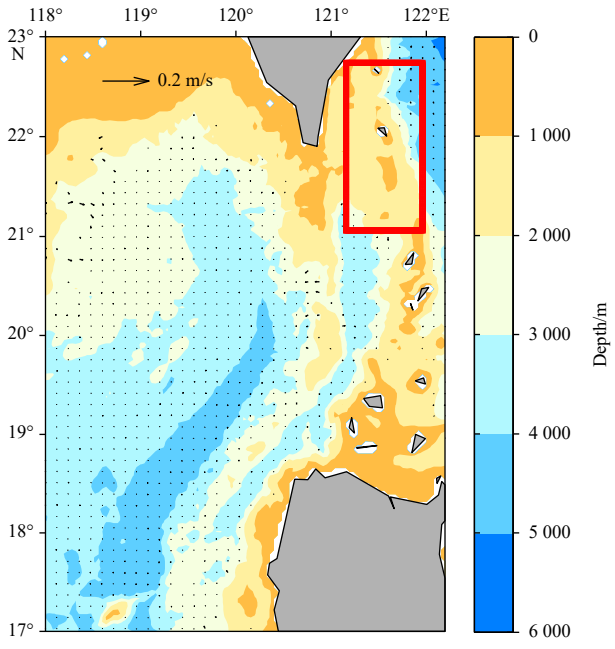

Fig. 7. The NHYCOM_produced Luzon Strait deep circulation in the topography modified experiment. In the red box, the channel at greater than 1 500 m depth in the eastern ridge of the Luzon Strait is closed.

tumn (October), after removing the Luzon Strait deep overflow, the SCS deep circulation in the northern part of the SCS deep basin almost disappeared, while the SCS deep circulation in the southern part of the SCS deep basin remained anti-cyclonic. In winter (January), without the Luzon Strait deep overflow, the SCS deep circulation significantly changes, resulting in a northward current along the western boundary, forming a basin-scale anti-cyclonic circulation. Lan et al. (2015) closed the whole Luzon Strait and obtained the basin-scale anti-cyclonic circulation in the winter, which was supportive of our conclusion. However, they also obtained basin-scale anti-cyclonic circulation in summer, which is different from ours results. The reason may be that the upper and intermediate water exchanges through the Luzon Strait as well as surface flux can also affect the SCS deep circulation and its seasonal variations.

In conclusion, after removing the Luzon Strait deep overflow, the SCS deep circulation amplitude is greatly weakened. Therefore, the Luzon Strait deep overflow is an important factor affecting the seasonal variation in the SCS deep circulation. Based on the PV-integral constraint, the dynamic mechanism of the effects of the Luzon Strait deep overflow on the seasonal variation in the SCS deep circulation can be explained. To ensure the PV balance, the PV inputted by Luzon Strait deep overflow should be dissipated by the frictional torque in the SCS deep basin. Therefore, the seasonal variation in the SCS deep circulation is significantly influenced by the Luzon Strait deep overflow.

5.2 *The role of the SCS surface wind*

Strong vertical mixing promotes the interaction between the upper circulation and deep circulation (Yuan, 2002; Wang et al., 2012; Yang, 2015). And the SCS upper circulation is mainly affected by the SCS surface wind (Yan, 1997). Therefore, the SCS surface wind may also be able to influence the SCS deep circulation through upwelling/downwelling. Another reason for exploring the influence of surface wind on the SCS deep circulation is based on the research of Tang et al. (2020). According to Tang et al. (2020), the large-scale phenomenon in the ocean is mainly induced by external forcings. The SCS deep circulation belongs to large scale phenomenon, so it is meaningful to study whether the external surface forcing can influence the SCS deep circulation.

To explore the influence of the SCS surface wind on the SCS deep circulation, a wind sensitivity experiment is designed by removing the SCS surface wind. Figs 3i–l show the NHYCOM_produced monthly mean SCS deep circulation in the wind sensitivity experiment. By comparing the control experiment with the wind sensitivity experiment, the SCS deep western boundary current in winter (January) is strongly affected by the SCS surface wind (Fig. 3i red box). In the control experiment, the SCS deep circulation in winter (January) is a through-flow structure from northeast to southwest across the central SCS deep basin, without an obvious deep western boundary current (Fig. 3a). However, in the wind sensitivity experiment, the SCS deep circulation in winter (January) shows a cyclonic structure, with a strong southward current along the western boundary. In the other seasons, after removing the SCS surface wind, the pattern of the SCS deep circulation does not change significantly, but the speed weakens to some extent.

Figure 8 shows the difference in monthly mean meridional velocity between the control experiment and the wind sensitivity experiment (at a depth of 3 000 m). The obvious difference in the meridional velocity appears along the western boundary of the SCS deep basin from October to the following February. The obvious positive meridional velocity difference at the western boundary of the SCS deep basin starts in October and then continues to increase, reaching a peak (approximately 1.5 cm/s) in December. After December, it begins to decrease and is negligible by the following March. Therefore, the influence of the SCS surface wind on the SCS deep western boundary current occurs mainly in winter, while in the remaining months, the influence is small.

Figure 9 shows the SCS deep western boundary current transport (below 2 000 m depth) contributed by the Luzon Strait deep overflow (gray bar) and by the SCS surface wind (white bar). The transport contributed by the Luzon Strait deep overflow is defined as the transport difference between the control experiment and the topography modified experiment. The transport contributed by the SCS surface wind is defined as the transport difference between the control experiment and the wind sensitivity experiment. Here, the western boundary current transport is defined as the average value of the cross-section transport of the two section (shown in Fig. 4). From March to September, the transports contributed by the SCS surface wind and by the Luzon Strait deep overflow are both southward, and the former transport is smaller. From October to the following February, the northward transport contributed by the SCS surface wind (average 1.2×10^6 m^3/s) is roughly equal to the southward transport contributed by the LZ deep overflow (average 1.40×10^6 m^3/s); thus, they offset each other.

In summary, the SCS surface wind influences the SCS deep circulation, especially during winter. In winter, at the western boundary of the SCS deep basin, the Luzon Strait deep overflow contributes a southward transport, while the SCS surface wind contributes a northward transport. The superimposed effect makes the SCS deep circulation a through-flow pattern without a western boundary current in winter. In summer, the current induced by the SCS surface wind in the deep western boundary is southward and weak, the Luzon Strait deep overflow still maintains the southward western boundary current, and the total SCS deep circulation is cyclonic. Combined with the results in Section 5.1, we can conclude that the SCS deep circulation pattern is mainly controlled by the Luzon deep overflow, and the SCS surface wind can significantly influence the SCS deep circulation in a specific season: winter. To some extent, our results are consistent with the analytical results of Wang et al. (2018), since they found that the spatial pattern of upwelling has a strong impact on the regional structures of the deep water circulation in the interior basin, but the overall basin scale circulation pattern is mainly controlled by the Luzon overflow.

The dynamic mechanism of the effects of the SCS surface wind on the seasonal variation of the SCS deep circulation is complex. Here, because of the lack of sufficient observational data, we cannot provide a full explanation for this dynamic mechanism. However, based on previous studies, some hypotheses and discussions can be given here. The first hypothesis is the meridional overturning circulation (Shu et al., 2014; Zhu et al., 2016). There are three meridional overturning circulations (MOCs) in the vertical SCS basin. These three MOCs can influence each other though vertical mixing. The upper MOC is mainly influenced by the SCS surface wind. Therefore, the influence of the SCS surface wind can directly influence the deep circulation through vertical mixing. The second hypothesis is Rossby waves. Figure 10 shows the Hovmoeller diagram of the daily mean 27.52 kg/m^3 isopycnal depth difference between the control experiment and the wind sensitivity experiment for 16°N (Fig. 10). The 27.52 kg/m^3 isopycnal depth is approximeatly 2 000 m in the SCS basin, roughly equivalent to the upper interface of

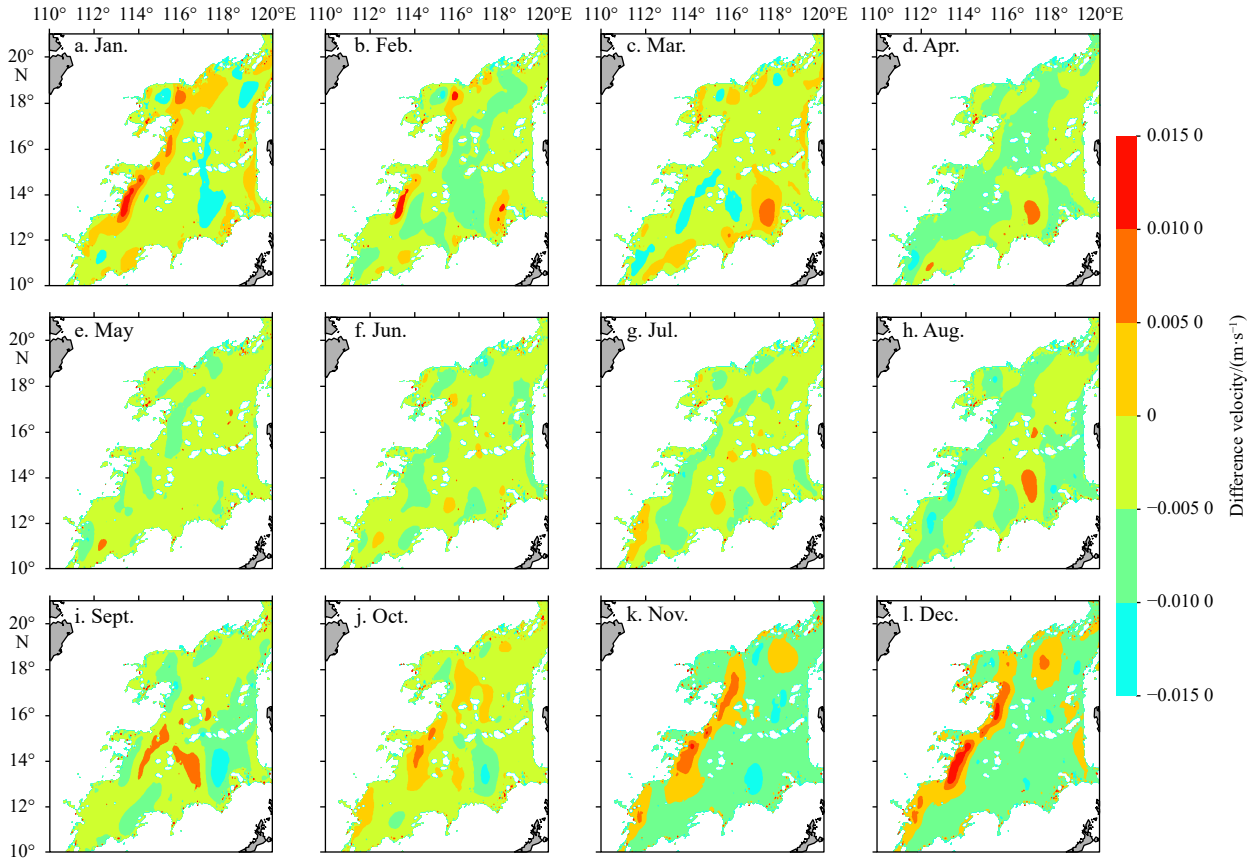

Fig. 8. The difference in monthly mean meridional velocity between the control experiment and the wind sensitivity experiment (control-sensitivity, at a depth of 3 000 m).

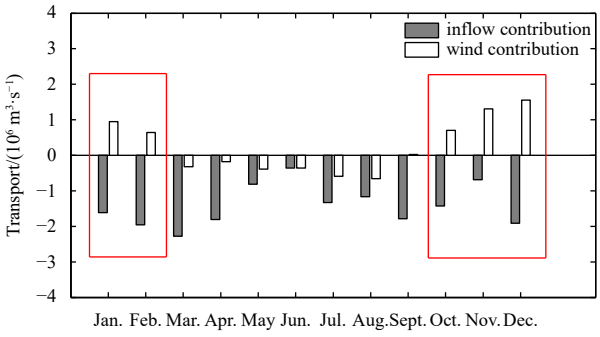

Fig. 9. The SCS deep western boundary circulation transport (below 2 000 m depth) was contributed by the Luzon Strait deep overflow (gray bar) and by the SCS surface wind (white bar). The positive value represents northward transport, and the negative value represents southward transport.

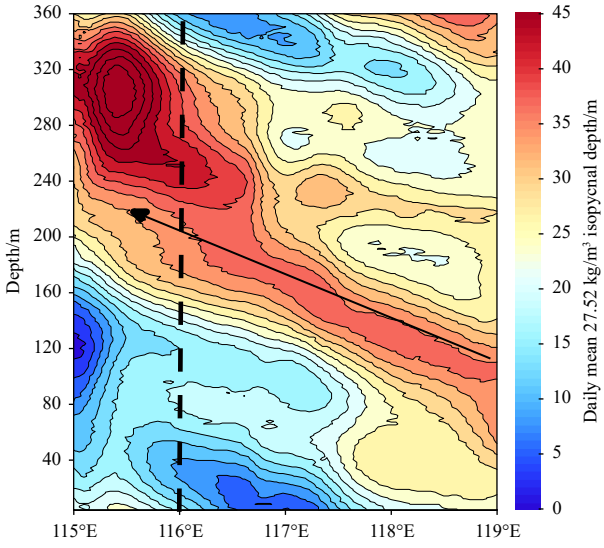

Fig. 10. The Hovmueller diagram of the daily mean 27.52 kg/m^3 isopycnal depth difference between the control experiment and the wind sensitivity experiment for 16°N. The black arrows show the signs propagating from the eastern boundary to the western boundary. Here, the area west of 116°E is defined as the western boundary.

the SCS deep water. In the figure, we can see that the signals contributed by the surface wind take approximately 3 months to propagate from the eastern boundary to the western boundary, which is consistent with the results of Shu et al. (2014), who found that those signals are the first-mode baroclinic Rossby wave in the SCS. In Fig. 9, the deep western boundary circulation transport contributed by the surface wind is at its maximum in December. This may be because the seasonally reversed monsoon signal that appeared in September excited the Rossby wave in the deep eastern boundary, and then took approximately 3 months to propagate to the deep western boundary and influence the deep western boundary circulation. The third plausible but intuitive hypothesis is based on the scale dependency of the signal-to-noise ratio in the SCS. Tang et al. (2020) found that at

large scales, the variability in the model output is mainly induced by external forcings and the proportion of the internal variability is small, so the signal-to-noise ratio is large. This result is not only confine in the upper ocean, but also a large scale phenomenon in the deep circulation. Therefore, deep circulation may also be influenced by external forcings, such as surface wind.

6 Conclusions

Using a two-level nested model, a high-resolution SCS deep circulation was obtained. The sensitivity model experiments were designed to independently study each potential impact factor impacting the SCS deep circulation. Based on the model results, some results of the seasonal variation of the SCS deep circulation and its deep western boundary current are described as follows.

(1) The SCS deep circulation and its western boundary current have obvious seasonal variation. By comparing the model results with the 41-year climatological monthly mean SODA2.2.4 data, the SCS deep circulation is found to be a basin-scale cyclonic structure with a strong southward deep western boundary current in summer (July) and is a northeast-southwest throughflow pattern across the central deep basin without a deep western boundary current in winter (January), while spring (April) and autumn (October) are transitional.

(2) The Luzon Strait deep overflow is an important factor affecting the seasonal variation of the SCS deep circulation. There are obvious seasonal variations in the Luzon Strait deep overflow. The transport is 0.6810^6–1.83×10^6 m^3/s, reaching its maximum in summer (July, up to 1.83×10^6 m^3/s), less in autumn and winter, and the lowest value occurs in spring (May, 0.68×10^6 m^3/s). The existence and seasonal variation in the Luzon deep overflow can be qualitatively estimated by the PV dissipation in the SCS deep basin.

(3) The SCS surface wind significantly influences the SCS deep circulation in winter. In winter, the joint effect of the Luzon Strait deep overflow and the SCS surface wind makes the SCS deep circulation a through-flow pattern without a western boundary current.

(4) The PV dissipation in the SCS deep basin reaches its maximum (-0.12 m^2/s^2) in May and its minimum (-0.38 m^2/s^2) in July.

Acknowledgements

Thanks should be given to China National Super computing Center in Jinan for providing the computing resources. We also thank Xiaoming Zhai for reading the manuscript and gave some good suggestions for us to improve this work. The COADS data used as the model forcing comes from the HYCOM's official website, https://hycom.org/hycom. The GEBCO data used as the model topography comes from the General Bathymetric Chart of the Oceans, https://www.gebco.net. The SODA data used in this paper comes from the ASIA-PACIFIC DATA-RESEARCH CENTER, http://apdrc.soest.hawaii.edu/datadoc.

References

Baraille R, Filatoff N. 1995. Modèle shallow-water multicouches isopycnal de Miami. Rapport d' Etude, CMO/RE No 003/95

Bleck R, Smith L T. 1990. A wind-driven isopycnic coordinate model of the north and equatorial Atlantic Ocean: 1. Model development and supporting experiments. Journal of Geophysical Research: Oceans, 95(C3): 3273–3285, doi: 10.1029/JC095iC03p03273

Carton J A, Chepurin G, Cao Xianhe. 2000. A simple ocean data assimilation analysis of the global upper ocean 1950–95. Part II: Results. Journal of Physical Oceanography, 30(2): 311–326, doi: 10.1175/1520-0485(2000)030<0311:ASODAA>2.0.CO;2

Carton J A, Giese B S. 2008. A reanalysis of ocean climate using Simple Ocean Data Assimilation (SODA). Monthly Weather Review, 136(8): 2999–3017, doi: 10.1175/2007MWR1978.1

Carton J A, Giese B S, Grodsky S A. 2005. Sea level rise and the warming of the oceans in the Simple Ocean Data Assimilation (SODA) ocean reanalysis. Journal of Geophysical Research: Oceans, 110(C9): C09006, doi: 10.1029/2004JC002817

Chang Y T, Hsu W L, Tai J H, et al. 2010. Cold deep water in the South China Sea. Journal of Oceanography, 66(2): 183–190, doi: 10.1007/s10872-010-0016-x

Chao S Y, Shaw P T, Wu S Y. 1996. Deep water ventilation in the South China Sea. Deep Sea Research Part I: Oceanographic Research Papers, 43(4): 445–466, doi: 10.1016/0967-0637(96)00025-8

Gan Jianping, Li H, Curchitser E N, et al. 2006. Modeling South China Sea circulation: Response to seasonal forcing regimes. Journal of Geophysical Research: Oceans, 111(C6): C06034, doi: 10.1029/2005JC003298

Gan Jianping, Liu Zhiqiang, Hui R C. 2016. A three-layer alternating spinning circulation in the South China Sea. Journal of Physical Oceanography, 46(8): 2309–2315, doi: 10.1175/JPO-D-16-0044.1

Hirschi J J M, Blaker A T, Sinha B, et al. 2013. Chaotic variability of the meridional overturning circulation on subannual to interannual timescales. Ocean Science, 9(5): 805–823, doi: 10.5194/os-9-805-2013

Lan Jian, Wang Yu, Cui Fengjuan, et al. 2015. Seasonal variation in the South China Sea deep circulation. Journal of Geophysical Research: Oceans, 120(3): 1682–1690, doi: 10.1002/2014JC010413

Lan Jian, Zhang Ningning, Wang Yu. 2013. On the dynamics of the South China Sea deep circulation. Journal of Geophysical Research: Oceans, 118(3): 1206–1210, doi: 10.1002/jgrc.20104

Li Li, Qu Tangdong. 2006. Thermohaline circulation in the deep South China Sea basin inferred from oxygen distributions. Journal of Geophysical Research: Oceans, 111(C5): C05017, doi: 10.1029/2005JC003164

Liu Zhiqiang, Gan Jianping. 2017. Three-dimensional pathways of water masses in the South China Sea: A modeling study. Journal of Geophysical Research: Oceans, 122(7): 6039–6054, doi: 10.1002/2016JC012511

Pedlosky J. 1982. Geophysical Fluid Dynamics. Berlin: Springer-Verlag

Pedlosky J. 1996. Ocean Circulation Theory. Berlin: Springer-Verlag

Qu Tangdong, Girton J B, Whitehead J A. 2006. Deepwater overflow through Luzon Strait. Journal of Geophysical Research: Oceans, 111(C1): 311–330, doi: 10.1029/2005JC003139

Shu Yeqiang, Xue Huijie, Wang Dongxiao, et al. 2014. Meridional overturning circulation in the South China Sea envisioned from the high-resolution global reanalysis data GLBa0.08. Journal of Geophysical Research: Oceans, 119(5): 3012–3028, doi: 10.1002/2013JC009583

Sun Jia, Wang Guihua, Zuo Juncheng, et al. 2017. Role of surface warming in the northward shift of tropical cyclone tracks over the South China Sea in November. Acta Oceanologica Sinica, 36(5): 67–72, doi: 10.1007/s13131-017-1061-8

Tang Shengquan, von Storch H, Chen Xueen, et al. 2019. "Noise" in climatologically driven ocean models with different grid resolution. Oceanologia, 61(3): 300–307, doi: 10.1016/j.oceano.2019.01.001

Tang Shengquan, von Storch H, Chen Xueen. 2020. Atmospherically forced regional ocean simulations of the South China Sea: Scale dependency of the signal-to-noise ratio. Journal of Physical Oceanography, 50(1): 133–144, doi: 10.1175/JPO-D-19-0144.1

Tian Jiwei, Qu Tangdong. 2012. Advances in research on the deep South China Sea circulation. Chinese Science Bulletin, 57(24): 3115–3120, doi: 10.1007/s11434-012-5269-x

Tian Jiwei, Yang Qingxuan, Liang Xinfeng, et al. 2006. Observation of

Luzon Strait transport. Geophysical Research Letters, 33(19): L19607, doi: 10.1029/2006GL026272

Wang Aimei, Du Yan, Peng Shiqiu, et al. 2018. Deep water characteristics and circulation in the South China Sea. Deep Sea Research Part I: Oceanographic Research Papers, 134: 55–63, doi: 10.1016/j.dsr.2018.02.003

Wang Guihua, Huang Ruixin, Su Jilan, et al. 2012. The effects of thermohaline circulation on wind-driven circulation in the South China Sea. Journal of Physical Oceanography, 42(12): 2283–2296, doi: 10.1175/JPO-D-11-0227.1

Wang Dongxiao, Xiao Jingen, Shu Yeqiang, et al. 2016. Progress on deep circulation and meridional overturning circulation in the South China Sea. Science China Earth Sciences, 59(9): 1827–1833, doi: 10.1007/s11430-016-5324-6

Wang Guihua, Xie Shangping, Qu Tangdong, et al. 2011. Deep South China Sea circulation. Geophysical Research Letters, 38(5): L05601, doi: 10.1029/2010GL046626

Xie Qiang, Xiao Jingen, Wang Dongxiao, et al. 2013. Analysis of deep-layer and bottom circulations in the South China Sea based on eight quasi-global ocean model outputs. Chinese Science Bulletin, 58(32): 4000–4011, doi: 10.1007/s11434-013-5791-5

Yan Junyue. 1997. Climatological characteristics on the onset of the South China Sea southwest monsoon. Acta Meteorologica Sinica, 55(2): 174–186

Yang Jiayan. 2005. The arctic and subarctic ocean flux of potential vorticity and the Arctic Ocean circulation. Journal of Physical Oceanography, 35(12): 2387–2407, doi: 10.1175/JPO2819.1

Yang Jiayan. 2015. Local and remote wind stress forcing of the seasonal variability of the Atlantic Meridional Overturning Circulation (AMOC) transport at 26.5°N. Journal of Geophysical Research: Oceans, 120(4): 2488–2503, doi: 10.1002/2014JC010317

Yang Jiayan, Price J F. 2000. Water-mass formation and potential vorticity balance in an abyssal ocean circulation. Journal of Marine Research, 58(5): 789–808, doi: 10.1357/002224000321358918

Yang Jiayan, Price J F. 2007. Potential vorticity constraint on the flow between two basins. Journal of Physical Oceanography, 37(9): 2251–2266, doi: 10.1175/JPO3116.1

Yuan Dongliang. 2002. A numerical study of the South China Sea deep circulation and its relation to the Luzon Strait transport. Acta Oceanologica Sinica, 21(2): 187–202

Zhao Wei, Zhou Chun, Tian Jiwei, et al. 2014. Deep water circulation in the Luzon Strait. Journal of Geophysical Research: Oceans, 119(2): 790–804, doi: 10.1002/2013JC009587

Zhao Xiaolong, Zhou Chun, Zhao Wei, et al. 2016. Deepwater overflow observed by three bottom-anchored moorings in the Bashi Channel. Deep Sea Research Part I: Oceanographic Research Papers, 110: 65–74, doi: 10.1016/j.dsr.2016.01.007

Zhou Chun, Zhao Wei, Tian Jiwei, et al. 2014. Variability of the deep-water overflow in the Luzon Strait. Journal of Physical Oceanography, 44(11): 2972–2986, doi: 10.1175/JPO-D-14-0113.1

Zhou Chun, Zhao Wei, Tian Jiwei, et al. 2017. Deep western boundary current in the South China Sea. Scientific Reports, 7: 9303, doi: 10.1038/s41598-017-09436-2

Zhu Yaohua, Fang Guohong, Wei Zexun, et al. 2016. Seasonal variability of the meridional overturning circulation in the South China Sea and its connection with inter-ocean transport based on SODA2.2.4. Journal of Geophysical Research: Oceans, 121(5): 3090–3105, doi: 10.1002/2015JC011443